ICANS-XI International Collaboration on Advanced Neutron Sources
KEK, Tsukuba, October 22-26, 1990

Single crystal diffraction at ISIS

C C Wilson and D A Keen
ISIS Facility, Rutherford Appleton Laboratory, Chilton, Didcot, Oxon OX11 0QX, UK.

ABSTRACT
The ISIS Single Crystal Diffractometer SXD is a time-of-flight Laue instrument. The utilisation of large area position-sensitive detectors along with the pulsed nature of the ISIS beam makes SXD an ideal instrument for reciprocal space surveying, measuring large volumes in a single scan. The development of detectors for SXD will be described along with data processing strategies, and illustrations given of the scientific programme.

I. INTRODUCTION

There is a rich variety of information available from single crystal diffraction at a pulsed neutron source. The utilisation of both the time-of-flight technique to sort the white beam and large area position-sensitive detectors makes it possible to access large volumes of reciprocal space in a single measurement. The ISIS Single Crystal Diffractometer SXD (Figure 1; Forsyth and Wilson, 1990) is just such a time-of-flight Laue instrument. The main features of SXD are evident from this figure and the parameters given in Table 1. The ability of such an instrument to probe reciprocal space volumes is illustrated in Figure 2. The combination of a time-sorted wavelength range (providing two Ewald sphere surfaces at $1/\lambda_{max}$ and $1/\lambda_{min}$) and the large scattering locus subtended by the detector, allows the area shown in Figure 2 to be accessed *in a single measurement*. Of course, the detector also has height, and a full 3-dimensional reciprocal space volume is accessed on SXD.

It is clear from the above that SXD is an ideal instrument for the surveying of reciprocal space. This capability has particular relevance in the study of incommensurate structures, phase transitions and diffuse scattering. In these fields the time-of-flight Laue technique is extremely powerful. However, the characteristics of the data collected on such an instrument can also have certain advantages in more routine structural work. For example in the treatment of wavelength dependent effects and in obtaining high precision refinements from very high $\sin\theta/\lambda$ data.

II. DETECTORS

The requirements for an efficient detector for single crystal diffraction at a pulsed spallation neutron source such as ISIS are rather stringent. The technique of Laue time-of-flight diffraction produces a very large amount of information accessible in principle to an area detector at one time. The polychromatic nature of the incident beam allows many Bragg reflections (> 1000 in many cases) to diffract simultaneously into a 300 x 300 mm^2 active area during an ISIS pulse. Since SXD is situated close to the moderator (L_1 = 8 m) this leads to a high flux and large count rate requirements. With much of the ISIS flux being at fairly short wavelengths in the epithermal region, it is clear that a PSD installed on the instrument must have good response to neutrons with wavelengths down to say 0.2 Å. Finally, some of the effects being looked for in single crystal diffraction, such as satellite reflections, require good resolution in all three dimensions, two spatial and one time.

In order to exploit the possibilities of SXD one therefore requires a PSD with good pixel resolution (at worst 5 mm), fast count rate (dead time ~1 μs), linearity of response and stability. The original detector developed for SXD is the Anger camera (Forsyth, Lawrence and Wilson, 1988; Wilson and Zaleski, 1990). In addition, more recent developments of fibre-optic encoded PSDs have led to the provision of prototype modules of this design on SXD with great success.

Figure 1 – Plan view of SXD. Note the provision of large area PSDs subtending a large scattering angle at the sample.

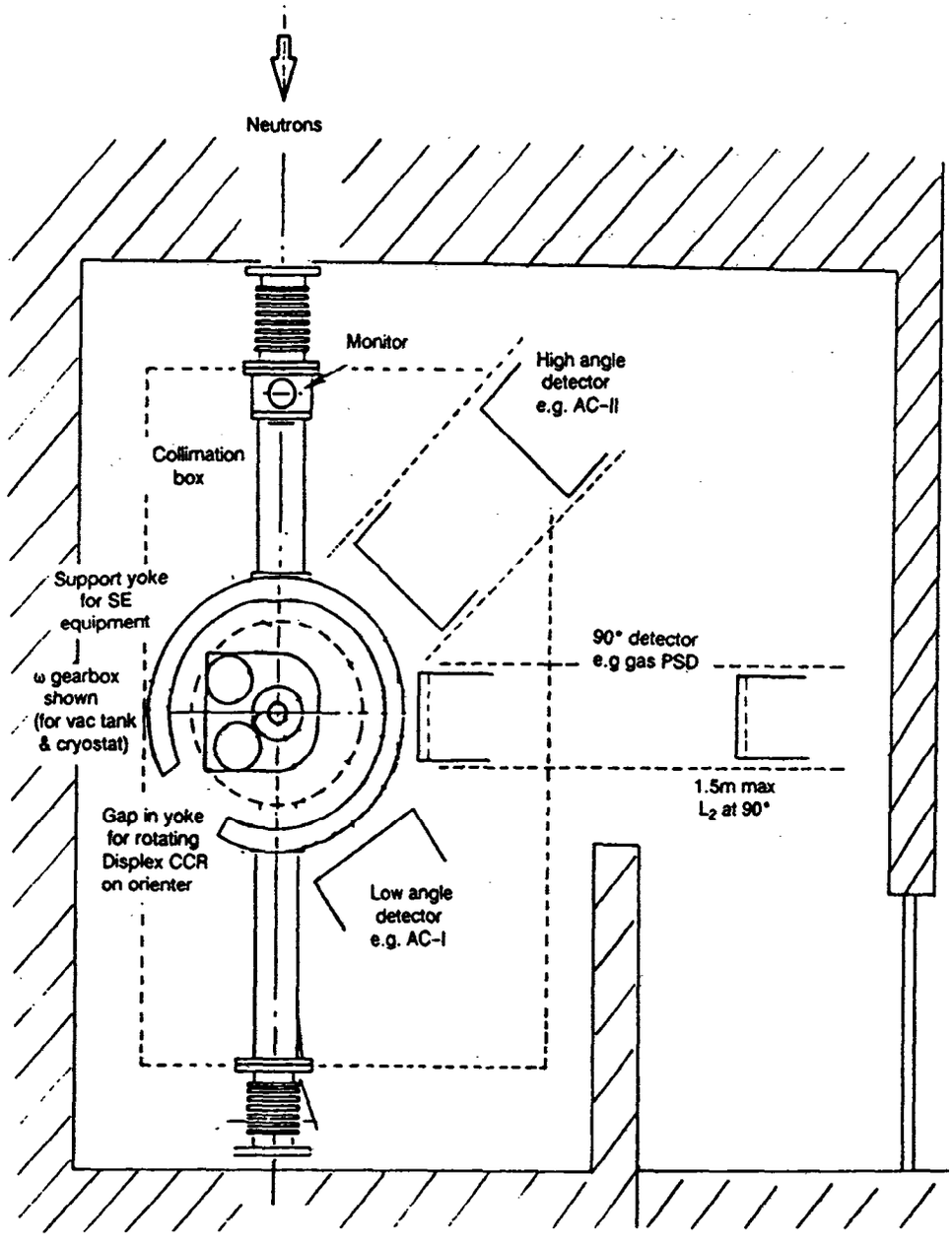

TABLE 1 – SXD instrument parameters

Laue time-of-flight diffractometer
Primary flight path $L_1 = 8$m from 316K H_2O moderator
Sample-detector distance $L_2 = 0.2$–1.5m (longest at 90°)
Wavelength range 0.25–8Å
$\sin\theta/\lambda$ range 0.02–2.5Å^{-1}

Detectors
Position-sensitive detectors

Fibre-optic encoded ZnS module, 80 x 80 mm^2, 5mm resolution
Anger camera I, ZnS scintillator, >300 x 300mm^2, 7–8mm resolution
Anger camera II in testing, ZnS scitnillator, >350 x 350mm^2, 5mm resolution
ORDELA ^{3}He gas detector, 250 x 250mm, 2–8mm resolution

Resolution, $\Delta d/d = 10^{-2} - 5.10^{-3}$

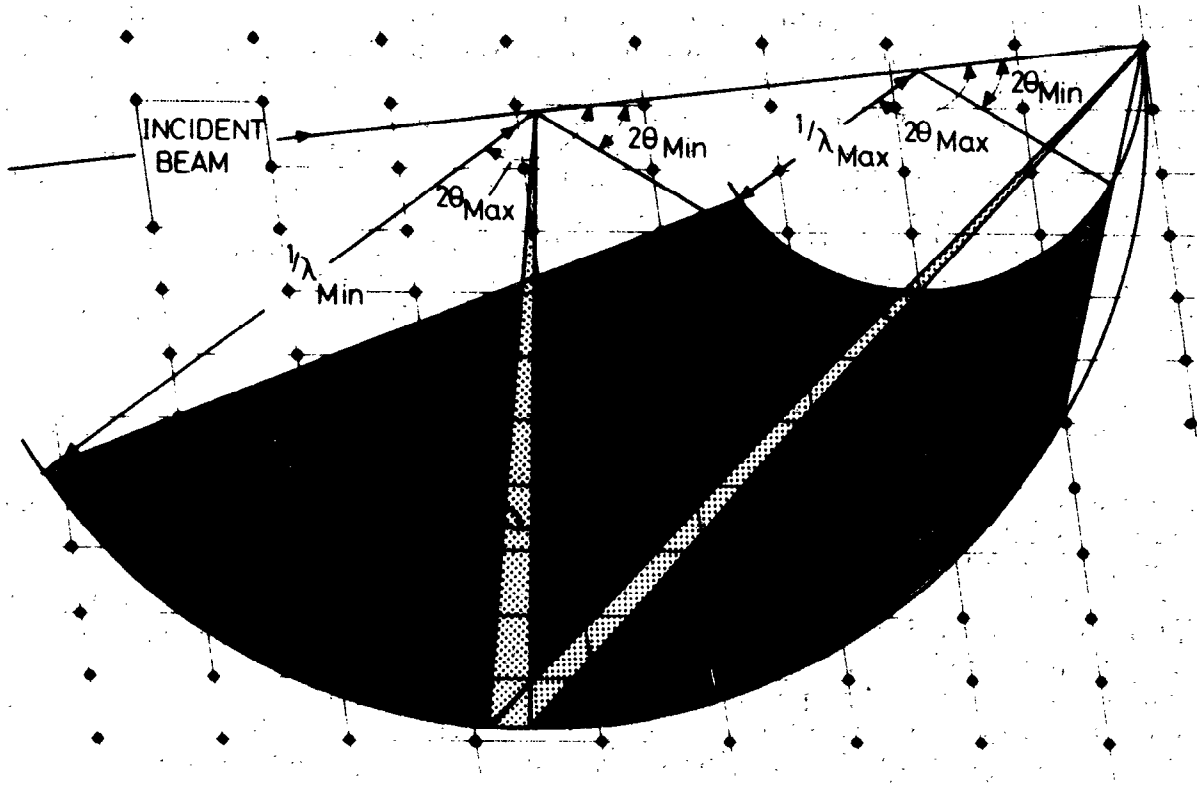

Figure 2 – Single crystal time-of-flight geometry

Anger Camera

The basic concept of this type of PSD (Anger, 1957) is that a single piece of scintillator is used to detect events. The light produced from an event is dispersed into an array of PM tubes (Figure 3) and the analogue signals of these tubes are used to derive electronically the position of the detected neutron. These detector coordinates would produce a 2D array of data were only positional information required but the addition of time-of-flight information on SXD produces a full 3D data set.

Figure 3 – General design of the neutron Anger camera.

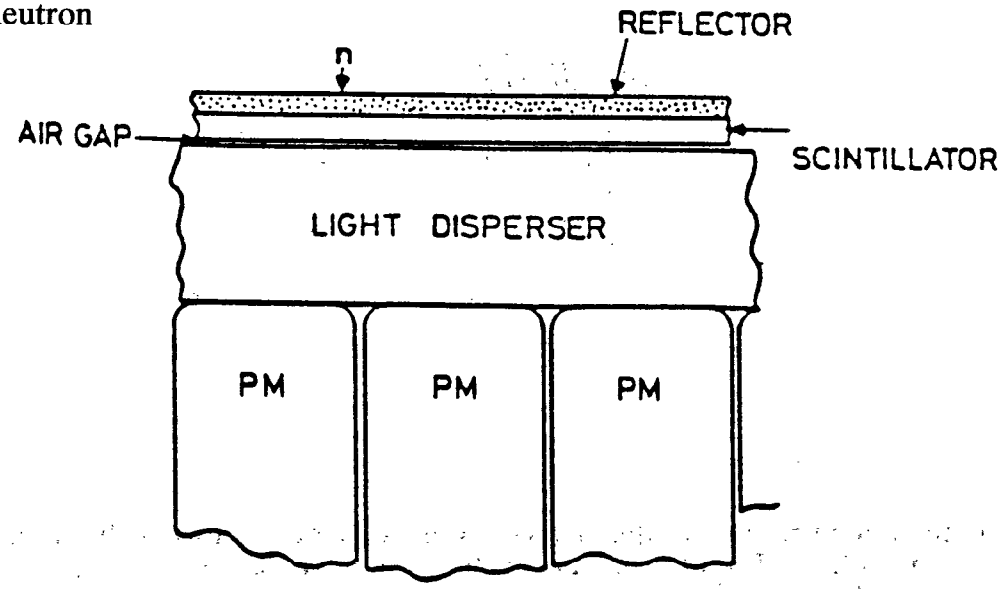

In the course of early commissioning of the Anger camera system, it was concluded that the available resolution was limited by the amount of light available from the optics, and also that the high γ sensitivity of the ^{6}Li-doped glass scintillator was causing considerable noise problems. Both of these problems can be overcome by the use of ^{6}Li loaded ZnS plastic scintillator, and it was found to be straightforward to modify the electronics to encompass the different dynamic response of this type of scintillator. The testing of the new AC-ZnS system was very successful. The resolution obtained from the prototype system is some 6-7 mm, but at present the count rate in the encoding electronics is rather slower than expected, a problem which is under investigation. With this caveat, however, it is the successful commissioning of the AC-ZnS system (Wilson and Zaleski, 1990) which has recently enabled the SXD scientific programme to begin in earnest.

The prototype fibre-optic ZnS PSD

The problems encountered with the Anger camera, and the re-examination of detector parameters in the light of experience on SXD, has prompted the examination of a new type of detector which is simpler both in concept and construction and is also less expensive to build. The fibre-optic ZnS PSD installed on SXD is a prototype constructed by the Neutron Detector group at ISIS (Davidson, Mott, Rhodes and Johnson, 1989). Basically the detector, shown schematically in Figure 4, consists of an array of 5 x 5 mm^2 pixel elements arranged on a ceramic grid, fibre-optic encoded to a set of phototubes. Physically, these pixel elements comprise inverted pyramids, abutted to form an array. The scintillator, a single, continuous piece of ~ 0.4 mm thick ^{6}Li-doped ZnS plastic, is supported some 0.1 mm above the base of these pyramids, with a group of optical fibres at each pyramid apex to collect the light and transmit this to the PMTs. In the prototype there are 16 x 16 pixels in X and Z, requiring 32 phototubes, giving an active area of some 80 x 80 mm^2. It has been shown that, by judicious choice of discriminator levels, this system can be made virtually insensitive to γ noise.

Figure 4 - General design of the prototype fibre-optic encoded ZnS PSD

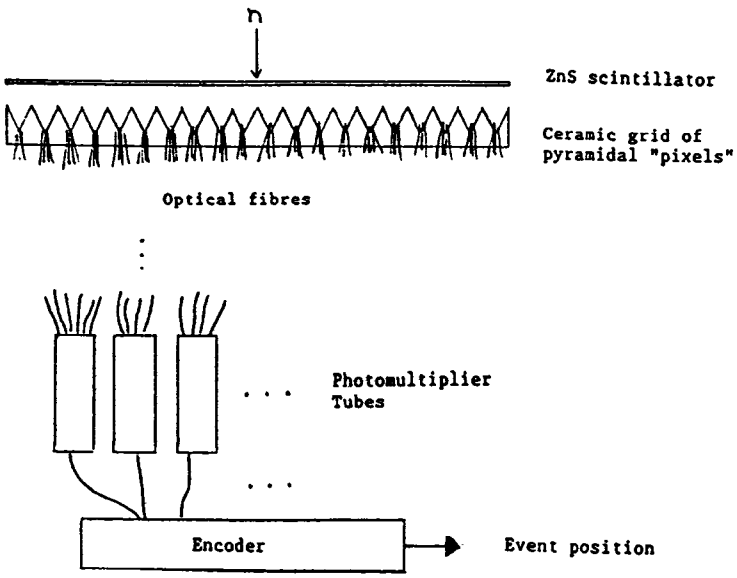

The commissioning results on this detector were very satisfactory with parameters found as illustrated in Table 2. The performance of this prototype detector has been excellent, and in spite of its small size, it has contributed significantly to the early stages of the SXD user programme.

TABLE 2 - ZnS fibre-optic PSD performance

Active area	80 x 80 mm^2 (typically subtending 20x20° at the sample)
Pixel resolution	5 mm x 5 mm
Linearity	Excellent to 0.1 mm
Quiet counts/detector noise	4 counts/cm^2/hour
Detector response	Smooth (flat) to < 10% and stable
Signal-to-background	> 4000:1 in (2 2 2) of SrF_2
Short wavelength response	(0 0 24) of SrF_2 observed at d = 0.24 Å, $\sin\theta/\lambda$ = 2.1$Å^{-1}$, Q = 26.4$Å^{-1}$
Dead time	2-3 μs
Stability and reliability	Robust, easy to install and operate.

Gas detector

In addition to the in-house detectors described, we have purchased a 2D ^{3}He gas PSD from ORDELA Inc. at Oak Ridge to supplement the detector array. This detector is still being commissioned, but should give spatial resolution in the range 2-8mm as a result of parallax caused by finite thickness of the gas volume. The availability of several detectors improves the flexibility of SXD and, in addition, provides PSDs to support the increasing programme of high resolution single crystal studies on HRPD.

III. SXD SOFTWARE: THE DUAL ROLE OF THE INSTRUMENT

The trouble with large volumes of reciprocal space is that in examining them, one obtains large volumes of diffraction information (scattered intensity measurements). SXD typically operates with several thousand detector elements (a single Anger camera has 64x64 pixels = 4096 detector elements), which when combined with a few hundred time channels, essential of course within the framework of the time-of-flight technique, tends to give rather large data histograms, each of which is typically accumulated in less than an hour. Hence a major requirement for the efficient exploitation of the technique is the availability of a flexible software package for data analysis and display (Forsyth et al, 1986).

SXD is designed, as far as possible, in accordance with standard 4-circle geometry, and is probably best defined as a "restricted 4-circle" diffractometer. As a consequence, the diffraction geometry can be defined by the equation of Busing and Levy (1967),

$$h_L = \Omega\, \chi\, \Phi\, \mathbf{U}\, \mathbf{B}\, h$$

where

h_L is the diffraction vector in the laboratory Cartesian system;
Ω, χ and Φ are the matrices defining the diffractometer settings;
U and **B** are matrices describing the sample;
h is the reciprocal lattice vector.

It is clear from this that once the UB matrix for the sample has been determined, the problem is well-defined and the data processing can be made fairly automatic. The SXD software package is illustrated in Figure 5, showing the central role of the UB matrix.

The dual purpose of SXD is evident in the portion of this Figure beyond UB matrix refinement. The left-hand path "Structural Refinement" is routine crystallographic work, involving the extraction of structure factors and subsequent least squares refinement, while the right-hand side "Reciprocal Space Surveying" attempts to exploit the special ability of a time-of-flight Laue diffractometer such as SXD to sample large reciprocal space volumes.

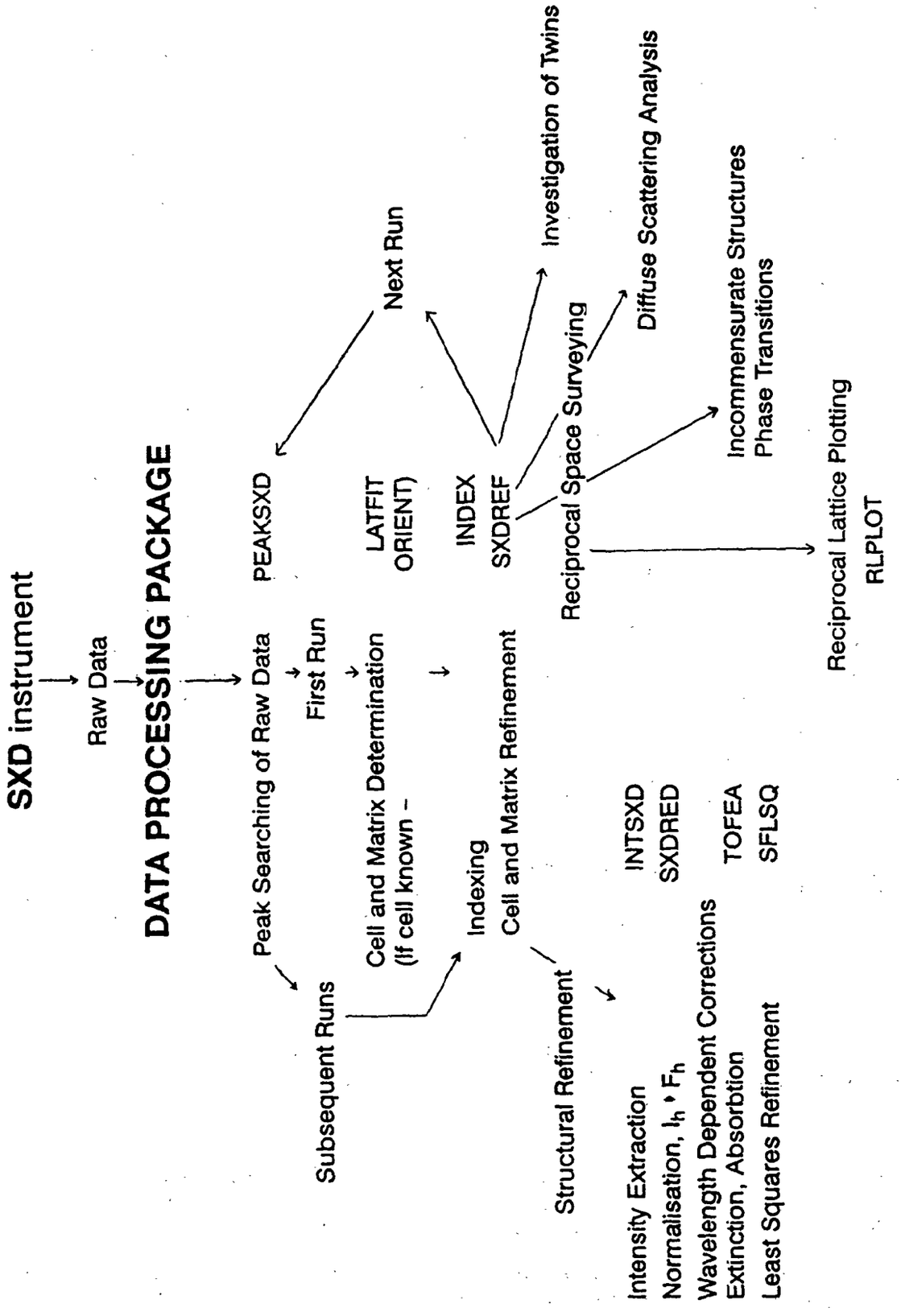

Figure 5 – The SXD data processing package.

IV. STRUCTURAL REFINEMENT

The extraction of structure factor information from an SXD data set proceeds in two stages. Given the provision of an accurate UB matrix from the earlier stages of the software package, integrated intensities are extracted from the raw data using Wilkinson's modification of the σ(I)/I method (Wilkinson, 1986; Wilkinson et al, 1988). Once a reliable set of integrated intensities has been extracted from the raw data, these are reduced to structure factors. This reduction includes calculation of the coefficients for the evaluation and subsequent refinement of wavelength and path length dependent absorption and extinction corrections, using routines from the Cambridge Crystallographic Subroutine Library (CCSL; Brown and Matthewman, 1987). Structure factor refinement is then carried out within the framework of CCSL using the least squares program SFLSQ.

Structure and disorder in schultenite

One of the first examples of successful "routine" structural refinement carried out on SXD is the study of $PbHAsO_4$ (Wilson, Cox and Stewart, 1990). Lead hydrogen arsenate, occurring naturally as the mineral schultenite, undergoes a paraelectric–ferroelectric phase transition at 313 K, manifest in a lowering of crystal symmetry from P2/c to Pc and a gradual ordering of the hydrogen bonded H atom onto one of two disordered sites. The separation of these H...H disordered positions along with the O...O separation in the hydrogen bond have great bearing on the nature of the H potential. A structure determination performed at room temperature on SXD using a sample provided by the British Museum clearly revealed the presence of this H atom, previously unlocated by X-rays, and its 50:50 occupancy over two disordered sites (Figure 6). The separation of the two hydrogen sites (0.388(19) Å) is in good agreement with that in related materials. The provision of such details in hydrogen bonded systems is a good example of the structural refinement aspect of the SXD programme. The data for this study extended to $\sin\theta/\lambda$ of $> 1\text{Å}^{-1}$, relatively high for such materials. This high resolution data allowed the refinement of the small distortion of the heavy atom lattice in the Pc phase. Further examination of these effects is in progress.

Figure 6 – High symmetry structure of $PbHAsO_4$, showing hydrogen atom disorder.

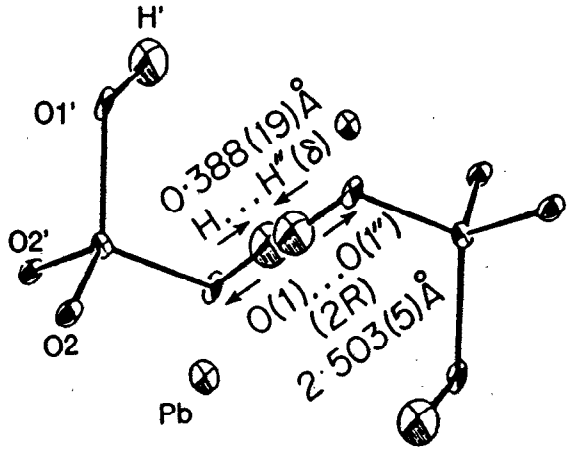

Wavelength dependent extinction and anharmonic thermal vibrations in strontium fluoride
The study of anharmonic thermal vibrations in SrF_2 (Forsyth, Wilson and Sabine, 1989) provided a rigorous test of the precision available from SXD. The data, from a heavily extinguished sample, provided a good example of the application of variable wavelength extinction corrections in CCSL. The extinction corrected data yielded an R-factor of 4.4% on those reflections expected to exhibit the effects of anharmonic vibrations of the fluorine atoms. The application of a third order anharmonic term, β_F, in the flourine potential led to a reduction in R-factor to 2.2%, and a value of $\beta_F = -4.19(30)\ 10^{-19}$ J Å^{-3}. this value was in good agreement with, but more precise than, the earlier $\beta_F = -3.95(46)\ 10^{-19}$ J Å^{-3} of Cooper and Rouse (1971). The improved precision is a consequence of the high $\sin\theta/\lambda$ value of 1.7 Å^{-1} reached on SXD (compared to 0.9 Å^{-1} in the earlier study).

V. RECIPROCAL SPACE SURVEYING

The other aspect of SXD, indicated on the right hand side of Figure 5, is to fully exploit the reciprocal space volumes accessed by the instrument in a single measurement. The ability to probe routinely those regions of reciprocal space *between* Bragg peaks lends the time-of-flight Laue technique great power in the study of incommensurate structures, phase transitions and diffuse scattering. Examples of the use of SXD in these cases are discussed below.

The simplicity of reciprocal space surveying on SXD again arises from the straightforward application of equation (1). In this case, one chooses a Q region (i.e. a set of indices $h_{min} < h < h_{max}$, $k_{min} < k < k_{max}$, $l_{min} < l < l_{max}$) within which one wishes to probe, with application of the equation as written giving the necessary detector coordinates to allow the data to be accessed. In the SXD package this is accomplished within the RLPLOT routines. Of course a mapping of reciprocal space points onto detector coordinates will never be exact and interpolation is adopted within the extraction program. Increased flexibility is also available within RLPLOT from the optional ability for performing detector and/or incident flux normalisation.

Diffuse scattering from Yttria-stabilised Zirconia
Within the cubic structure of Zirconia (ZrO_2), which is stabilised at ambient temperature by the presence of >9mol% Yttria (Y_2O_3), oxygen vacancies exist to maintain electrical neutrality. While the structure of ZrO_2/Y_2O_3 is fluorite, within the crystal there occur vacancy-free regions which cause a slight tetragonal distortion of the cubic lattice. This effect will give rise to coherent diffuse peaks at systematically absent Bragg peak positions. In addition, there is some ordering of vacancy pairs within the structure, giving rise to superlattice diffuse peaks in positions away from the Bragg peaks.

Figure 7 shows data collected on SXD from a single crystal of ZrO_2-9.4%Y_2O_3 (Hull et al, 1990). The sample was aligned with $<1\bar{1}0>$ vertical, allowing access to (hhl) reflections in the equatorial plane of the detector. The figure shows this (hhl) section, and clearly shows Bragg and diffuse scattering from this material. The sharp reflections such as (113) and (224), with h,k,l all even or all odd, are allowed in the cubic space group. Others, such as (114) and (116), are the diffuse Bragg peaks due to the distortion of the cubic lattice. There is also some diffuse scattering in the regions away from the Bragg peak positions, the observation of which is made easier by the surveying capability of SXD. These superlattice peaks are those caused by vacancy clustering. The measurement of diffuse scattering to the high Q values accessible on SXD (note the observation of the (1,1,10) diffuse peak) is important for the reliable modelling of the structural disorder causing this intensity.

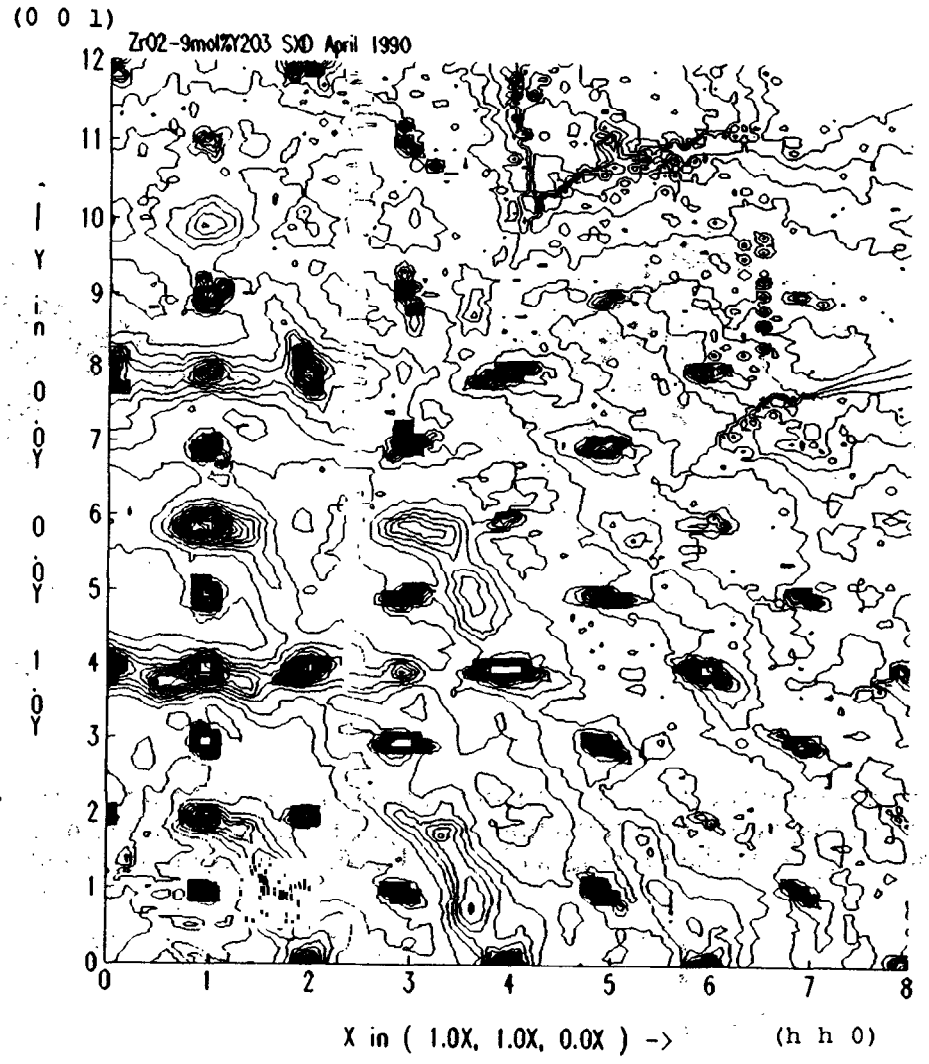

Figure 7 – Bragg and diffuse scattering in the (hhl) plane of yttria-stabilised zirconia, ZrO_2–9.4%Y_2O_3. Note the high Q reached in this measurement, with the (1,1,10) diffuse peak clearly visible.

Magnetic phase transition in Holmium

The low temperature diffraction pattern of Holmium is rich in magnetic structure. The reciprocal space scanning properties of SXD can be used to follow phase transitions such as that in Ho (at around 133K) in a particularly simple way. By retaining the crystal and detector geometry fixed in one orientation it is possible to measure the temperature dependence of many reflections simultaneously. Satellite reflections, their positions and intensities, can be examined in any direction in reciprocal space. In an experiment such as the one in this example, one SXD histogram is frequently sufficient to give all the required data under one set of sample conditions.

In this experiment (Stirling et al, 1990), the region around (00l) was examined in the temperature range 150 → 14K. The magnetic phase transition gives rise to incommensurate reflections at (0,0,l±q) which can clearly be seen to appear as the temperature is lowered from 150K to 120K. Figures 8a and 8b show the (0kl) reciprocal lattice plane of Ho measured above and below the magnetic phase transition, clearly demonstrating the appearance of incommensurate satellite peaks. The temperature variation of the (00l) row clearly showed the satellites to move closer to the Bragg peaks and lock-in at $q = 1/6c$. In addition to these measurements around (00l), full scans of the (h0l) plane were carried out at a series of temperatures in the magnetically ordered region. These surveying scans, carried out rapidly and conveniently on SXD show, as expected, no evidence of squaring of the magnetic satellite structure (Figure 9).

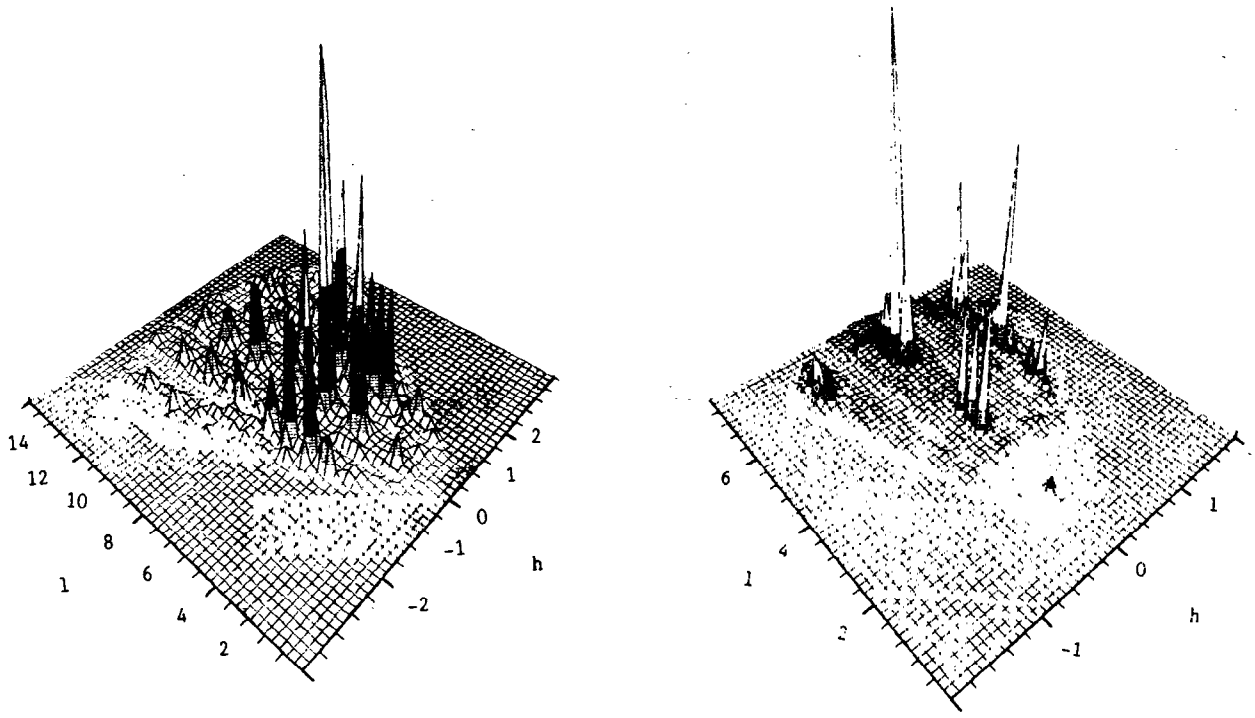

Figure 8 – Reciprocal lattice plots of sections of the (0kl) plane in Ho above (left) and below (right) the magnetic phase transition. The appearance of satellites in the low temperature phase is apparent. Note the Q–ranges displayed in these plots are different.

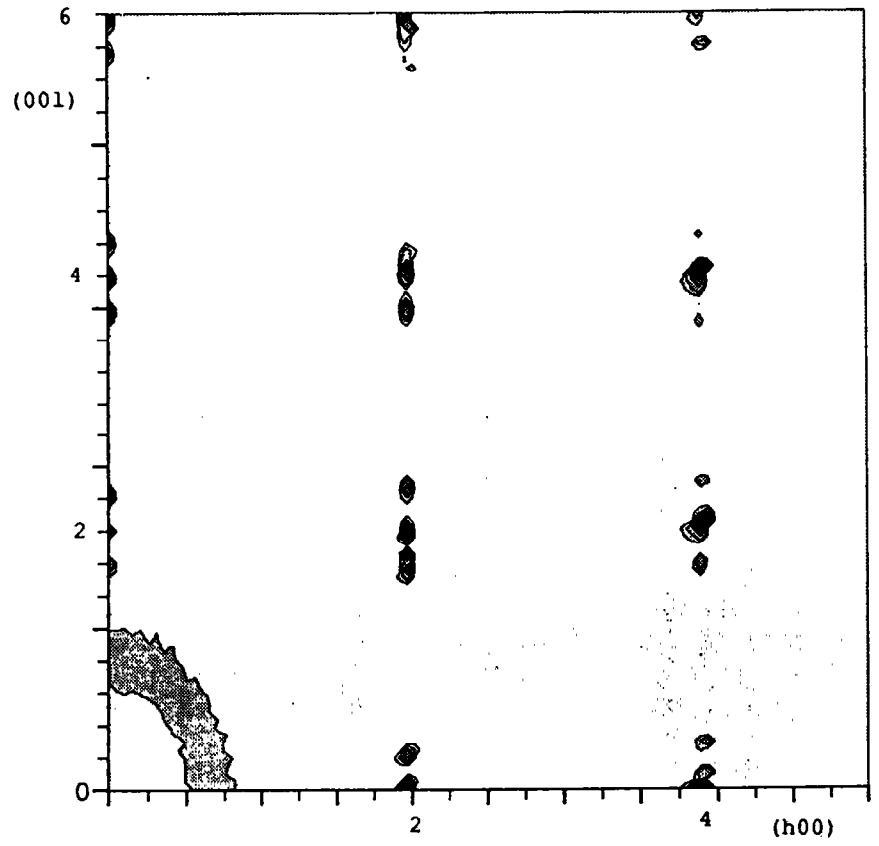

Figure 9 – A projection of the (h0l) plane in Ho at 120K showing the one dimensional nature of the incommensurate vector *q*, along *c*.

Ferroelastic domains in $LiKSO_4$

Lithium potassium sulphate undergoes several phase transitions, at temperatures varying from 940 to 38 K. These transitions have been characterised by several techniques, but for most of the phases only preliminary single crystal neutron scattering data are available. In both phase V below 198 K and phase VI below 38 K there is a ferroelastic domain structure leading to a broadening and splitting of certain peaks in the diffraction pattern. The study of this material on SXD should allow the measurement of peak shape in all reciprocal space directions and hence lead to a greater understanding of the symmetry changes involved in the paraelastic–ferroelastic phase transition. The profile of the $(1\bar{2}0)$ reflection of $LiKSO_4$ at 60K is shown in Figure 10. As can be seen from this, peak broadening and splitting is observed, showing the symmetry to drop at least to orthorhombic and possibly to monoclinic in phase V.

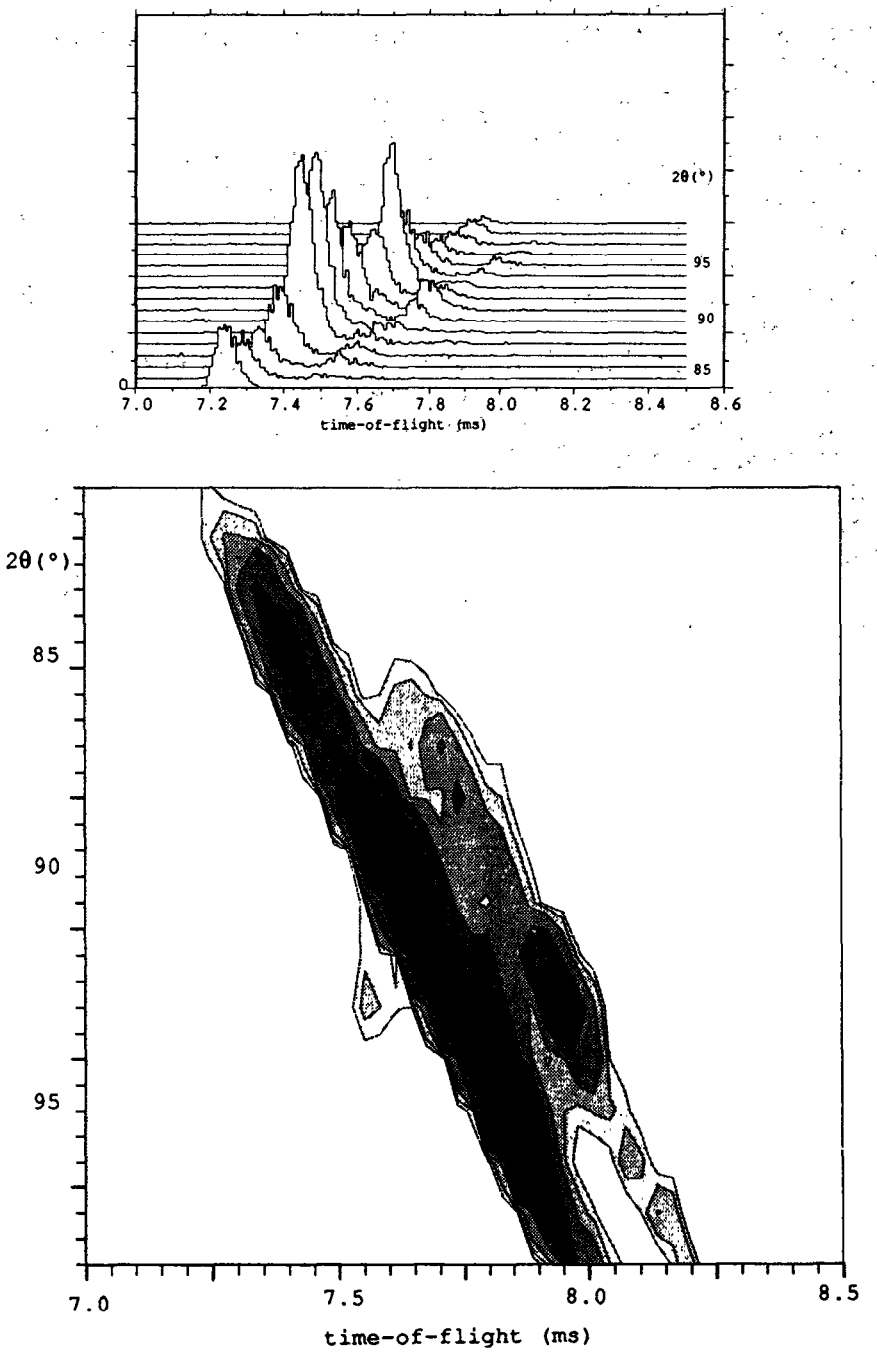

Figure 10 – The profile of the $(1\bar{2}0)$ reflection of $LiKSO_4$ at 60K, displayed as a multiplot of spectra and a contour plot in $(2\theta,t)$ space. The broadening and splitting of this peak, which is narrow and single above 190K, gives information on the ferroelastic domain symmetry.

VI. CONCLUDING REMARKS

It is clear from the results presented in these later sections that the first year or so of science performed on SXD have been rather successful and show great promise for the future, especially in the fields of diffuse scattering and reciprocal space probing. Developments of the detection system are continuing in parallel with the scientific programme, with the next aim to provide a larger version of the fibre-optic encoded ZnS module, the best and most reliable detection system available on SXD to date.

References

Anger H O, Rev. Sci. Insts. 29, 27 (1958)
Brown P J and Matthewman J C, Rutherford Appleton Laboratory Report, RAL-87-010 (1987)
Busing W R and Levy H A, Acta Cryst. 22, 457 (1967)
Cooper M J and Rouse K D, Acta Cryst. A27, 622 (1971)
Davidson P L, Mott E M, Rhodes N J and Johnson M W, in Advanced Neutron Sources 1988, ed D K Hyer, IOP Conference Series 97, 523 (1989)
Forsyth J B, Lawrence R T and Wilson C C, Nucl. Inst. Meth. A273, 741 (1988)
Forsyth J B and Wilson C C, to be published (1990)
Forsyth J B, Wilson C C, Stringer A M, Howard J A K and Johnson O, J. de Phys. Colloque C5-47, 143 (1986)
Forsyth J B, Wilson C C and Sabine T M, Acta Cryst. A45, 244 (1989)
Hull S, Goff J, Hutchings M T and Hayes W, to be published (1990)
Stirling W G, Tang C C, Haycock P W and Wilson C C, to be published (1990)
Wilkinson C, J. de Phys. Colloque C5-47, 35 (1986)
Wilkinson C, Khamis H W, Stansfield R F D and McIntyre G J, J. Appl. Cryst. 21, 471 (1988)
Wilson C C, Rutherford Appleton Laboratory Report RAL-89-014 (1989)
Wilson C C and Forsyth J B, Rutherford Appleton Laboratory Report RAL-89-005 (1989)
Wilson C C and Zaleski T, to be published (1990)